

Performance of the Expanded Virtual Point Transformation on a Complex Test Structure

Tomaž Bregar^a, Ahmed El Mahmoudi^c, Gregor Čepon^{b,*}, Daniel J. Rixen^c, Miha Boltežar^b

^a*Gorenje d.d., Partizanska 12, 3503 Velenje, Slovenia*

^b*Faculty of Mechanical Engineering, University of Ljubljana, Aškerčeva 6, 1000 Ljubljana, Slovenia*

^c*Technical University of Munich, Institute of Applied Mechanics, Boltzmannstr. 15, 85748 Garching, Germany*

Cite as:

Tomaž Bregar, Ahmed El Mahmoudi, Gregor Čepon, Daniel J. Rixen, Miha Boltežar, Performance of the Expanded Virtual Point Transformation on a Complex Test Structure, Experimental Techniques, 2020, <https://doi.org/10.1007/s40799-020-00398-1>

Abstract

The Virtual Point Transformation (VPT) makes it possible to experimentally identify the full DoF FRF matrix by projecting the measured displacements onto the Interface Deformation Modes (IDMs). The VP FRFs were already successfully used in Frequency-Based Substructuring (FBS); however, the VPT is susceptible to deviations in the impact location and orientation, as well as to deviations in the sensor's sensitivity and positioning. Uncertainties associated with the sensors can be decreased by using the expanded VPT. This expanded VPT allows the projection of a directly measured rotational response onto the Interface Deformation Modes (IDMs). The consistency of the transformation is achieved by using a rotational weighting matrix, which is formulated to minimize the norm of the overall displacements due to the rotational residual at the VP for each rotational sensor. The rotational response is measured using a direct piezoelectric rotational accelerometer. In this paper the application of the expanded virtual point transformation and the possible advantages are explored on a complex and engineering-like test structure. Both transformations, standard and expanded, are performed for each VP to enable a side-by-side comparison.

Keywords: frequency-based substructuring, expanded virtual point transformation, rotational accelerometer, interface rotation

1 Introduction

The Dynamic Substructuring (DS) framework makes it possible to dynamically characterize a complex product by subdividing it into smaller subsystems [1]. Each subsystem can then be analyzed independently and virtually assembled to predict the overall dynamics of the final product. This component-wise approach has proven to be advantageous, especially during the early design stage, when a full prototype might not be available. The dynamic characterization of each subsystem can be in different domains, such as the physical, modal, frequency, time or state-space domain [2]. Even with distinct differences between each representation, there are two conditions that must be satisfied at the interface between the substructures and are mathematically equivalent throughout the different domains. The first condition is displacement compatibility and the second is force equilibrium.

One of the frameworks where the numerical and experimental models can be coupled interchangeably is Frequency-Based Substructuring (FBS). The idea of frequency-based assembly was already

*Corresponding author

Email address: gregor.cepon@fs.uni-lj.si (Gregor Čepon)

considered in the early 70's [3, 4] and further elaborated by Jetmundsen et al. [5] at the end of the 80's. However, the limitations associated with the measurement equipment in that time rendered the application of the idea in practice difficult. This drawback stagnated the development until the beginning of the 21st century when the topic received a new attention and more systemic notations were developed, such as the Lagrange Multiplier FBS method (LM FBS) [6]. The main challenge with the FBS is the interface modelling and measuring full-degrees-of-freedom (DoF) Frequency Response Functions (FRFs). Coupling substructures in the FBS without the rotational DoF can lead to erroneous results [7]. Rotational DoFs are accessible from a numerical model; however, acquiring rotational DoFs from experimental measurements is still problematic, especially for the moment-excited part of the response.

The overall inaccessibility of the rotational DoF led to the development of several methods that implicitly measure and include rotations in the coupling procedure [7, 8]. One of the methods that include the Rotational Degrees of Freedom (RDoF) implicitly is the Equivalent Multi Point Connection (EMPC) [9]. With the EMPC method, multiple connection points are coupled to account for the rotational DoF and most of the time the interface problem is overdetermined.¹ With the excessive overdetermination of the interface even a small error can result in erroneous coupling results. The problem with EMPC overdetermination can be solved by IDM filtering, where the measured translation DoFs are projected onto the Interface Deformation Modes (IDMs) and with that a generalized set of displacements and forces is obtained in a minimal-quadratic sense [9, 10]. The IDM filtering is also known under the name of Virtual Point Transformation [11]. The transformation matrices in the VPT are determined from the positions of the sensors and impacts; however, even a small deviation in the positions can lead to a large error in the transformed FRFs. One way of decreasing the uncertainties associated with the positions of the accelerometers is using the expanded VPT, where a directly measured rotational response is included in the transformation [12]. The rotational response is measured with a rotational accelerometer [13].

The objective of this paper is to compare the performance of the standard VPT and the expanded VPT on a complex structure. For a better understanding, the next section briefly summarizes the LM FBS together with the VPT and an expansion where a directly measured rotational response is included in the transformation. Afterwards, the expanded VPT is compared with the standard VPT on a test structure representing a simpler version of an engine-transmission unit's suspension. A side-by-side comparison is made on a coupling example, where the source structure is coupled through rubber mounts to a receiver. In the final section a conclusion is drawn, together with general recommendations for the use of the expanded VPT.

2 Theory

With frequency-based substructuring the admittance of the assembled system can be determined from the separate admittances of the substructures. The governing equation of two non-assembled subsystems \mathbf{Y}^A and \mathbf{Y}^B can be written in block-diagonal form $\mathbf{Y}^{A|B}$, as follows:²

$$\mathbf{Y}^{A|B}(\mathbf{f} + \mathbf{g}) = \begin{bmatrix} \mathbf{Y}^A & \mathbf{0} \\ \mathbf{0} & \mathbf{Y}^B \end{bmatrix} (\mathbf{f} + \mathbf{g}) = \begin{bmatrix} \mathbf{u}^A \\ \mathbf{u}^B \end{bmatrix}, \quad (1)$$

where \mathbf{u} denotes the displacements, \mathbf{f} the external forces and \mathbf{g} the interface forces between the two substructures. To couple the substructures, two conditions must be satisfied at the interface. The first is the condition of compatibility ($\mathbf{u}_2^A - \mathbf{u}_2^B = \mathbf{0}$) and the second is the force equilibrium ($\mathbf{g}_2^A = -\mathbf{g}_2^B$), where the $(\star)_2$ refers to the interface DoF. Both conditions can be expressed with a

¹An interface is considered to be overdetermined when more DoF are included in the coupling than are in fact needed. Consider a perfectly rigid interface, where perfect coupling can be performed with only 6 DoFs (3 translation and 3 rotational). However, with the EMPC method one would need to use 3 triaxial translation accelerometers to account for the rotational DoFs. Therefore, the interface would be overdetermined.

²An explicit dependency on the frequency is omitted for the simplicity of the notation, and this will also be used for the remainder of the paper.

signed Boolean matrix \mathbf{B} and the substructures can then be coupled using the LM FBS notation [6]:

$$\mathbf{Y}^{\text{AB}}\mathbf{f} = \left(\mathbf{Y}^{\text{A|B}} - \mathbf{Y}^{\text{A|B}}\mathbf{B}^{\text{T}}(\mathbf{B}\mathbf{Y}^{\text{A|B}}\mathbf{B}^{\text{T}})^{-1}\mathbf{B}\mathbf{Y}^{\text{A|B}} \right)\mathbf{f} = \mathbf{u}. \quad (2)$$

The collocation of the interface DoF on both substructures was implicitly assumed in the LM FBS formulation. The collocation of the DoF at the interface is in reality inaccessible for an experimental setup, since neither the sensors nor the excitation points are collocated. Therefore, the substructures cannot be directly coupled using only the LM FBS.

2.1 Standard virtual point transformation

Collocation at the interface between the two substructures can be obtained using the Virtual Point Transformation (VPT) [11]. The VPT is a geometrical transformation where the measured translation DoFs are projected onto the interface deformation modes, which are assumed to properly describe the interface. The interface is usually assumed to be rigid; however, the rigid IDMs can be extended with the proper flexible interface modes [14].

After applying the transformation, a generalized set of displacements \mathbf{q} and generalized forces \mathbf{m} are obtained for each substructure:

$$\mathbf{Y}_{\text{qm}} = \mathbf{T}_{\text{u}}\mathbf{Y}_{22}\mathbf{T}_{\text{f}}^{\text{T}}, \quad (3)$$

where \mathbf{Y}_{22} denotes the non-collocated interface DoF, \mathbf{T}_{u} is the displacement transformation matrix and \mathbf{T}_{f} is the force transformation matrix. The set of generalized displacements \mathbf{q} is obtained in a minimal-quadratic sense:

$$\mathbf{q} = \mathbf{T}_{\text{u}}\mathbf{u} \quad \text{where} \quad \mathbf{T}_{\text{u}} \triangleq (\mathbf{R}_{\text{u}}^{\text{T}}\mathbf{W}_{\text{u}}\mathbf{R}_{\text{u}})^{-1}\mathbf{R}_{\text{u}}^{\text{T}}\mathbf{W}_{\text{u}}, \quad (4)$$

where \mathbf{u} denotes the measured interface displacements.³ The \mathbf{R}_{u} is the so-called IDM matrix, defined based on the IDMs and the positions of the sensors and the \mathbf{W}_{u} is a displacement weighting matrix used to assign a weighting to certain sensor channels in the error minimisation. In a similar way the force transformation matrix is defined with the matrix \mathbf{R}_{f} based on the IDMs and the positions of the impacts. Additionally, a diagonal weighting matrix is introduced \mathbf{W}_{f} :

$$\tilde{\mathbf{f}} = \mathbf{T}_{\text{f}}^{\text{T}}\mathbf{m} \quad \text{where} \quad \mathbf{T}_{\text{f}}^{\text{T}} \triangleq \mathbf{W}_{\text{f}}\mathbf{R}_{\text{f}}(\mathbf{R}_{\text{f}}^{\text{T}}\mathbf{W}_{\text{f}}\mathbf{R}_{\text{f}})^{-1}. \quad (5)$$

If the locations of the impacts and sensors were accurate and the interface was perfectly rigid, then the transformation would be perfect and with that also the generalized displacements and forces. However, the VPT has been shown to be affected by a rather small bias in the locations and orientations of the sensors as well as the impacts [11]. In the next section an expansion to the VPT is presented, where the directly measured rotational response is included in the transformation. The properties of the rotational accelerometer are expected to increase the overall robustness of the VPT and increase the consistency of the generalized DoF.

2.2 Expanded virtual point transformation

Rotational DoFs are essential for the coupling of substructures in the FBS. With the virtual point transformation, the rotational DoFs are estimated based on the prevailing assumption of local rigidity in the vicinity of the interface (provided that the locations of the sensors and impacts are known). However, the estimation of the sensor as well as the impact positions and orientations can only be determined up to a certain measurement accuracy [15]. The high sensitivity of indirect methods led to the development of a direct, quartz-based, piezoelectric, rotational accelerometer [13].

The rotational FRFs obtained from the rotational accelerometer are accurate and the sensor itself has a relatively low cross-axis sensitivity [16]. The use of a rotational accelerometer in the FBS

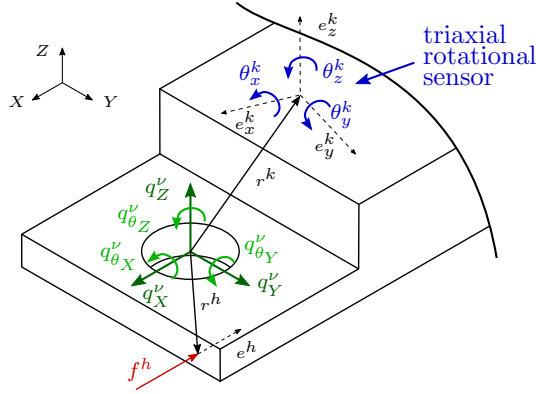


Figure 1: Interface example with virtual point and triaxial rotational sensor [12].

has already proven to be useful [17], which is one of the primary reasons behind the expansion of the virtual point transformation with a directly measured rotational response.

To derive the expansion, consider a relatively simple interface with a triaxial rotational accelerometer (Fig. 1). The following kinematic relation can be written between the virtual DoF \mathbf{q}^ν and the sensor rotation $\boldsymbol{\theta}^k$ [12]:

$$\begin{bmatrix} \theta_x^k \\ \theta_y^k \\ \theta_z^k \end{bmatrix} = \begin{bmatrix} e_{x,X}^k & e_{x,Y}^k & e_{x,Z}^k \\ e_{y,X}^k & e_{y,Y}^k & e_{y,Z}^k \\ e_{z,X}^k & e_{z,Y}^k & e_{z,Z}^k \end{bmatrix} \begin{bmatrix} 0 & 0 & 0 & 1 & 0 & 0 \\ 0 & 0 & 0 & 0 & 1 & 0 \\ 0 & 0 & 0 & 0 & 0 & 1 \end{bmatrix} \begin{bmatrix} q_X^\nu \\ q_Y^\nu \\ q_Z^\nu \\ q_{\theta_X}^\nu \\ q_{\theta_Y}^\nu \\ q_{\theta_Z}^\nu \end{bmatrix} + \begin{bmatrix} \mu_{\theta_x}^k \\ \mu_{\theta_y}^k \\ \mu_{\theta_z}^k \end{bmatrix}, \quad (6)$$

where $\boldsymbol{\mu}_\theta^k$ contains any residual motion, which can consist of the motion not spanned by the subspace of the IDMs, as well as any measurement error. A clear advantage of the expansion can be seen from the kinematic relation since the rotations depend only on the sensor orientation and not on the location of the sensor if the rigid assumption of the interface is valid. If we expand the formulation to include all the directly measured rotational responses we obtain:

$$\boldsymbol{\theta} = \mathbf{R}_\theta \mathbf{q} + \boldsymbol{\mu}_\theta. \quad (7)$$

Equation (7) can be combined with all the measured translation DoFs as follows:

$$\begin{bmatrix} \mathbf{u} \\ \boldsymbol{\theta} \end{bmatrix} = \begin{bmatrix} \mathbf{R}_u \\ \mathbf{R}_\theta \end{bmatrix} \mathbf{q} + \begin{bmatrix} \boldsymbol{\mu}_u \\ \boldsymbol{\mu}_\theta \end{bmatrix} = \mathbf{R}_{u,\theta} \mathbf{q} + \boldsymbol{\mu}_{u,\theta}. \quad (8)$$

Similar to the standard VPT the equation above can be solved for \mathbf{q} in a minimal-quadratic sense, where the norm of the weighted residuals on the displacements and rotations is minimized:

$$\mathbf{q} = \operatorname{argmin} \left(\begin{bmatrix} \boldsymbol{\mu}_u \\ \boldsymbol{\mu}_\theta \end{bmatrix}^T \mathbf{W}_{u,\theta} \begin{bmatrix} \boldsymbol{\mu}_u \\ \boldsymbol{\mu}_\theta \end{bmatrix} \right) \quad \text{where} \quad \mathbf{W}_{u,\theta} = \operatorname{diag}[\mathbf{W}_u, \mathbf{W}_\theta]. \quad (9)$$

If both weighting matrices \mathbf{W}_θ and \mathbf{W}_u are chosen as identity matrices the residuals are not evaluated in a comparable norm, since $\boldsymbol{\mu}_u \boldsymbol{\mu}_u^T \neq \boldsymbol{\mu}_\theta \boldsymbol{\mu}_\theta^T$. In order to evaluate both residuals in a comparable way, a proper weighting matrix for the rotations should be used [12].

The rotational weighting matrix can be defined by estimating the translation at the virtual point based on the residual rotation of each rotational channel. Presume that the rotational sensor k

³The sensors used for measuring the interface displacement \mathbf{u} are usually tri-axial accelerometers, but for the simplicity of the notation, displacements are considered here.

measuring rotation around the x axis has a residual $\mu_{\theta_x}^k$ (see Fig. 1). Based on the distance between the x axis across the VP and the sensor location, the displacement at the VP would be $\mu_{\theta_x}^k d_x^k$, where d_x^k denotes the aforementioned distance, which is equal to $\sqrt{r_y^2 + r_z^2}$. A similar weighting can be defined for all the other rotational channels and with that the rotational weighting matrix is defined as [12]:

$$\mathbf{W}_\theta = \text{diag} \left[(d_x^k)^2, (d_y^k)^2, (d_z^k)^2, \dots \right]. \quad (10)$$

With this weighting matrix, Eq. (7) can be solved for \mathbf{q} and the combined transformation matrix $\mathbf{T}_{u,\theta}$ is obtained:

$$\mathbf{q} = \mathbf{T}_{u,\theta} \begin{bmatrix} \mathbf{u} \\ \boldsymbol{\theta} \end{bmatrix} \quad \text{where} \quad \mathbf{T}_{u,\theta} \triangleq (\mathbf{R}_{u,\theta}^T \mathbf{W}_{u,\theta} \mathbf{R}_{u,\theta})^{-1} \mathbf{R}_{u,\theta}^T \mathbf{W}_{u,\theta}. \quad (11)$$

With this weighting matrix, the rotational and displacement residuals are minimized in a comparable norm. The positions of the rotational sensors are only used to define a proper norm for the least-square problem. Therefore, if the rotational measurement were perfect, the rotation of the VP would be defined exactly (notwithstanding any error in the position of the rotational sensors).

Note that a particular case for the rotational weighting matrix is when the rotational accelerometer is placed exactly at the VP location. Then the matrix \mathbf{W}_θ would become a zero matrix and the directly measured rotational response would be excluded from the transformation. Therefore, care should be taken not to place the rotational accelerometer in exactly the same position as the VP. This can almost always be achieved since the position of the VP near the interface is arbitrary, to a certain extent.

2.3 Measurement-quality indicators

One of the advantages of the VPT is also the ability to evaluate the quality of the transformation and the associated measurements by utilizing the assumption of interface rigidity. After the transformation, the virtual DoF can be expanded (or projected) back on the measured DoFs and with that the assumption of interface rigidity can be evaluated [11, 18]. Two different quality indicators can be calculated for the displacement/force transformation, which are the specific and overall sensor/impact consistency indicators [11]. With the consistency indicators, bad sensor channels or impact locations can be identified and removed from the transformation.

An additional quality indicator can be defined using the reciprocity property of the VP DoFs. Virtual point motions and loads are in fact collocated; therefore, the virtual point FRF matrix should be reciprocal. A coherence criterion can be used to evaluate the reciprocity of the VP DoFs per frequency line [18]:

$$\chi_{ij} = \text{coh}(Y_{ij}, Y_{ji}) = \frac{(Y_{ij} + Y_{ji})(\bar{Y}_{ij} + \bar{Y}_{ji})}{2(\bar{Y}_{ij} Y_{ij} + \bar{Y}_{ji} Y_{ji})}, \quad (12)$$

where i and j denote the different DoFs in the VP FRF matrix. The only limitation of reciprocity is that it can only be used on the non-diagonal entries, since on the diagonal the coherence is $\chi_{ii} = 1$ by definition. For the diagonal FRFs, the passivity can be evaluated since the driving-point FRFs should always be minimum-phase functions; therefore, the phase of the driving-point FRFs should always be bounded by $\angle Y_{ii} \in [0^\circ, 180^\circ]$ for accelerance FRFs.

The formulation of the expanded VPT does not affect the calculation of the quality indicators. Therefore, the sensor and impact consistency, as well as the reciprocity and passivity, can be used to evaluate the quality of both the standard and expanded transformations.

3 Application on a test-structure

This section demonstrates a practical application of the LM FBS using the standard and expanded virtual point transformation on the test structure shown in Fig. 2. The test structure is designed to mimic the dynamics in a real car of an engine unit flexibly mounted on a chassis. Rubber mounts from the automotive industry are used to suspend a steel plate holding the excitation source, which is an electrodynamic shaker. The structure is intended as a laboratory test bench for an application of different concepts of dynamic substructuring and transfer-path analysis [19].

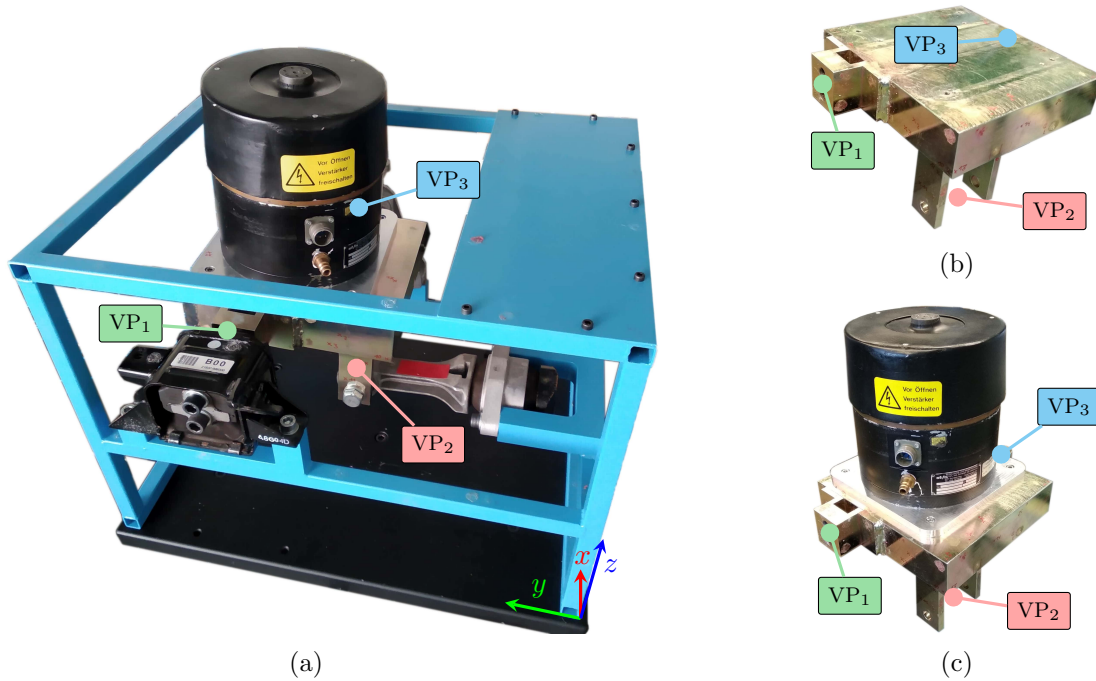


Figure 2: Test structure used for the comparison: a) assembly \mathbf{Y}^{AB} representing an engine-transmission unit suspension; b) transmission simulator \mathbf{Y}^{TS} ; c) source \mathbf{Y}^A representing the car engine.

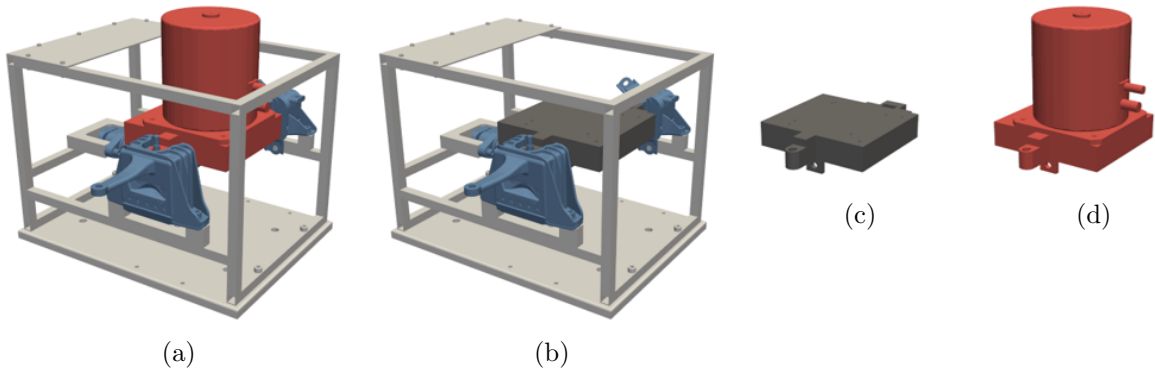


Figure 3: All measurement configurations of the test structure: a) assembly \mathbf{Y}^{AB} ; b) receiver with TS \mathbf{Y}^{BTS} ; c) transmission simulator \mathbf{Y}^{BTS} ; d) source \mathbf{Y}^A .

The coupling in this paper is between the source structure \mathbf{Y}^A (Fig. 3d) and the receiver structure \mathbf{Y}^B , which is the frame with the rubber bushings included (Fig. 3a without the source). However, the VPT measurements cannot be performed directly on the receiver side due to insufficient space to position sensors and impacts. A Transmission Simulator (TS) \mathbf{Y}^{TS} (Fig. 3c) is used to enable measurements around the rubber bushings [20]. Moreover, the numerical condition of the coupling procedure is increased, since the TS used has similar dynamic properties as the source structure and with that the receiver structure in the decoupled state, \mathbf{Y}^{BTS} (Fig. 3b), is behaving in a way

similar to that in the final assembled state, \mathbf{Y}^{AB} (Fig. 3a) [21]. Usually, a numerical model of the TS is used to increase the quality of the decoupling; however, with this setup, an experimental model of the TS was used. The final DS process can be represented with a simple equation, where the circled plus/minus sign denotes the coupling/decoupling procedure:

$$\mathbf{Y}^{AB} = \mathbf{Y}^{BTS} \ominus \mathbf{Y}^{TS} \oplus \mathbf{Y}^A, \quad (13)$$

where \mathbf{Y}^{BTS} denotes the assembly of structures \mathbf{Y}^B and \mathbf{Y}^{TS} .

3.1 Application of the VPT

The virtual point transformation was applied to all three experimental models \mathbf{Y}^{BTS} , \mathbf{Y}^{TS} and \mathbf{Y}^A . One virtual point for each rubber bushing was used, altogether three VPT were performed (see Fig. 2 and 4a). The rubber bushing at VP_1 represents the transmission mount, VP_2 is the rubber bushing at the roll mount and VP_3 is at the engine mount's rubber bushing.

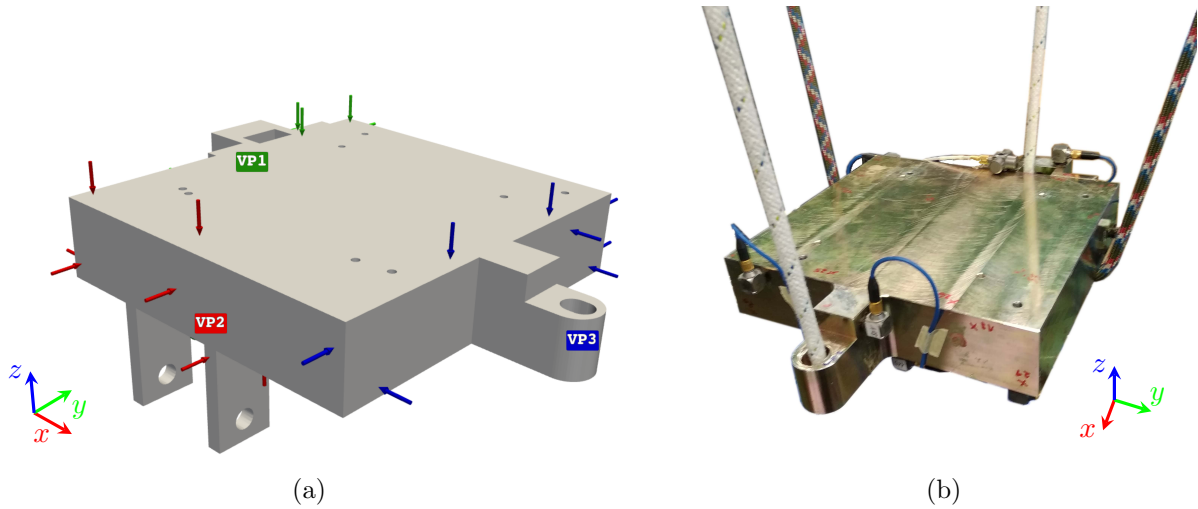


Figure 4: Transmission simulator structure: a) schematic representation of VPs together with visible impact locations depicted with arrows in different color for each VP; b) photograph of the experimental setup.

The final assembly structure \mathbf{Y}^{AB} (used as a reference) and \mathbf{Y}^{BTS} were rigidly fixed on a stiff and vibration-free test table during the measurements. The source \mathbf{Y}^A and transmission simulator \mathbf{Y}^{TS} were measured in a free-free condition (see Fig. 4b). All the FRFs were measured by impact testing using a modal hammer with a vinyl tip. For the standard VPT, three triaxial accelerometers (Kistler Type 8688A) were used and nine different impact locations for each VP. Altogether, 27 translation channels with 27 impact locations were used for the standard VPT.

A rotational accelerometer (Kistler Type 8840) was used to measure the rotational response for the extended VPT. The rotational accelerometer used measures only the rotation around one axis and only one rotational accelerometer was available for the whole measurement setup. Therefore, the rotational accelerometer was used as a roving sensor to acquire three rotational FRFs for each VP (as depicted in Fig. 5 for two directions).

The VPT was performed on all three experimental models; however, the results shown for the VPT quality in this section are only for the receiver structure with the TS \mathbf{Y}^{BTS} . The quality of both transformations can be estimated from the frequency-averaged coherence criterion for reciprocity depicted in Fig. 6. The average reciprocity of the standard VPT is 58%, while the expanded VPT with rotations has an average reciprocity of 61%.

The expanded VPT slightly outperforms the standard VPT, as can be seen from the average reciprocity criterion. A similar observation can be made if we compare the separate FRFs: in Fig. 7 the reciprocal transformed FRFs on \mathbf{Y}^{BTS} $VP_{1-y}/VP_{1-\theta_x}$ (2,4) and $VP_{1-\theta_x}/VP_{1-y}$ (4,2) are

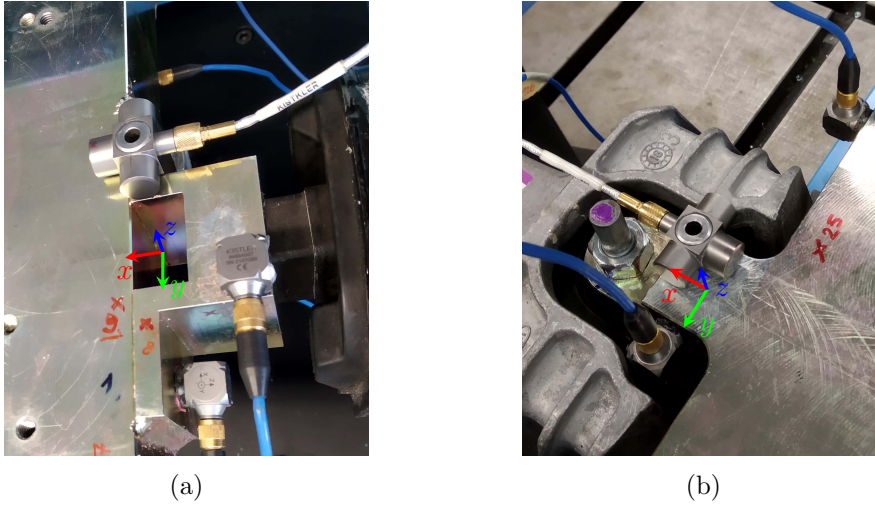


Figure 5: Positions of the rotational accelerometer: a) VP_1 direction $-RX$; b) VP_3 direction $+RX$.

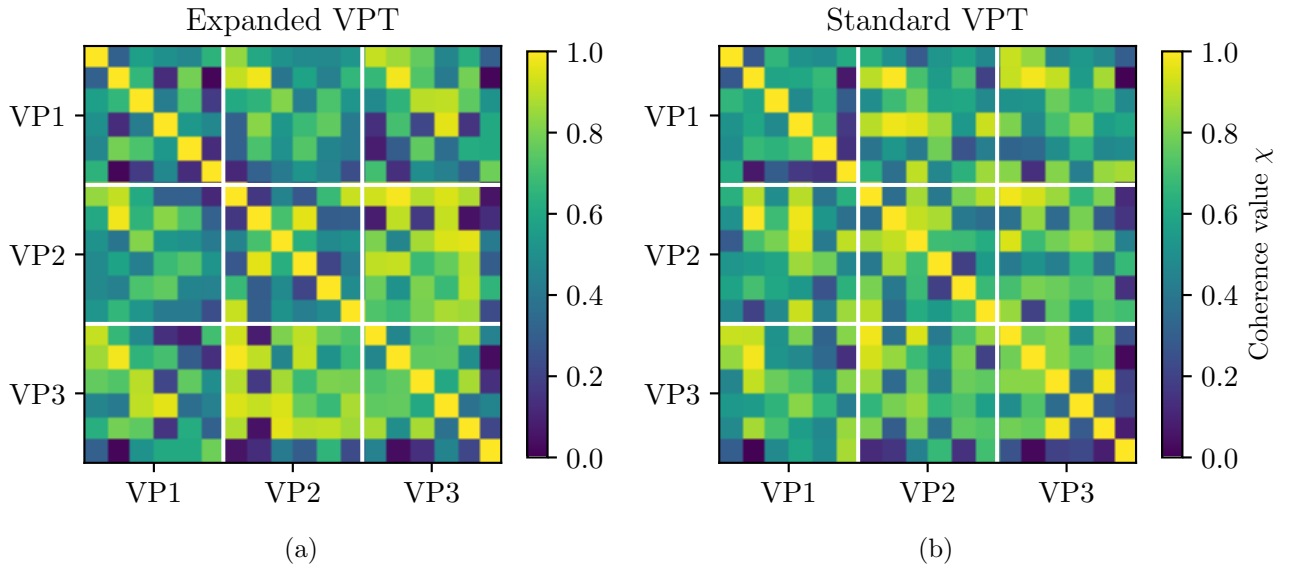


Figure 6: Frequency-averaged reciprocity of the VPT for all three virtual points of the receiver structure with the transmission simulator \mathbf{Y}^{BTS} : a) expanded VPT; b) standard VPT.

shown.⁴ The expanded VPT outperforms the standard in the higher frequency range and in the low-frequency range the FRFs obtained with the standard VPT are more reciprocal.

In Fig. 8 the transformed FRFs $VP_2-x/VP_3-\theta_z$ (7,18) and $VP_3-\theta_z/VP_2-x$ (18,7) are shown where the expanded VP FRFs are more reciprocal over the whole frequency range.

For both transformations a relatively high sensor and impact consistency was obtained (on average above 90% for the specific as well as for the overall consistency). Therefore, the positions and orientations of the impacts and sensors can be assumed to be accurate and the assumption of the interface rigidity in the frequency range of interest is satisfied. However, a high-quality VPT does not necessarily guarantee consistent coupling results. In the following section the final coupling results are presented and both transformations are compared.

3.2 Substructuring results

The final assembled system is shown in Fig. 9, where the positions of the reference sensors and impact positions also are depicted. The reference FRFs were measured in the assembled system to

⁴The first number in the bracket (2,4) refers to the output position and the second to the input position in the FRFs matrix i.e. (output,input).

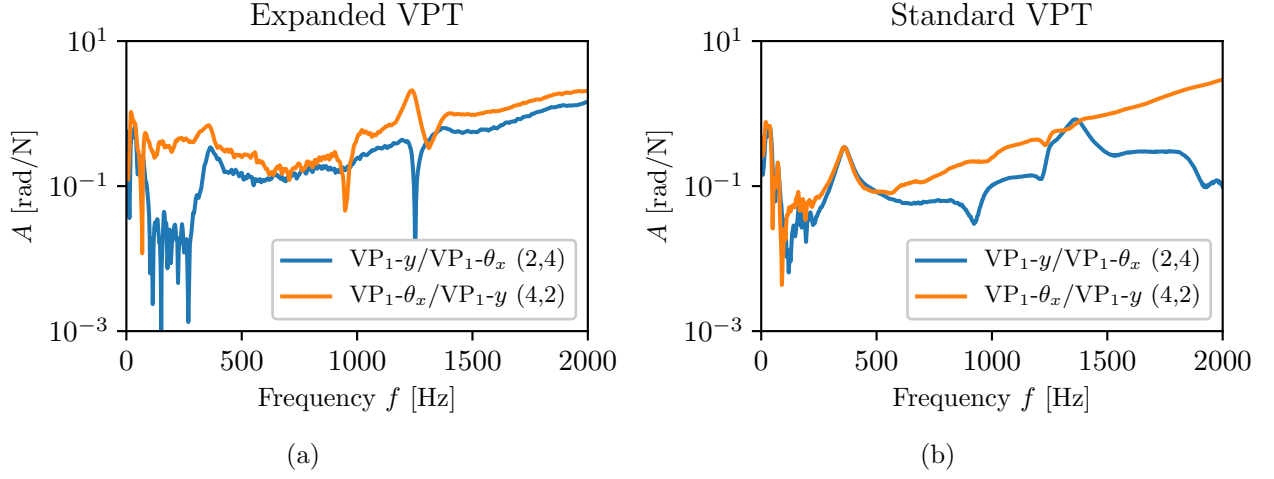


Figure 7: Comparison of specific virtual point FRFs $VP_{1-y}/VP_{1-\theta_x}$ (2,4) and $VP_{1-\theta_x}/VP_{1-y}$ (4,2) for the receiver structure with the transmission simulator \mathbf{Y}^{BTS} : a) expanded VPT; b) standard VPT.

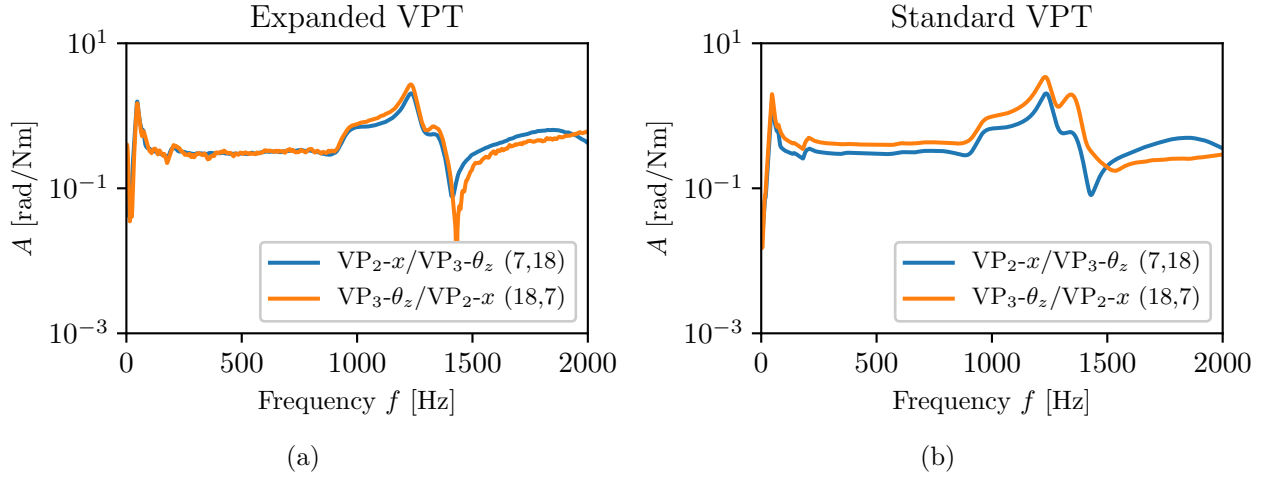


Figure 8: Comparison of the FRFs $VP_{2-x}/VP_{3-\theta_z}$ (7,18) and $VP_{3-\theta_z}/VP_{2-x}$ (18,7) for the receiver structure with the transmission simulator \mathbf{Y}^{BTS} : a) expanded VPT; b) standard VPT.

gain a reference with which the whole coupling procedure can be validated.

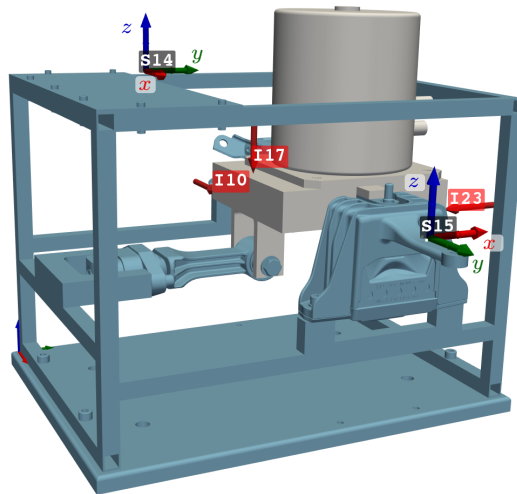


Figure 9: A view of the assembled system \mathbf{Y}^{AB} together with the reference sensors (denoted with letter S) and impact positions (denoted with letter I).

The coupling FRFs are obtained using the LM FBS notation. A signed Boolean matrix \mathbf{B} was used to define the interface DoF for the coupling and decoupling procedure. SVD truncation was used on the interface flexibility matrix \mathbf{Y}_{int} to remove the six smallest singular values before applying the matrix inversion in Eq. (2) to decrease the errors of the coupling procedure [22].⁵

In Fig. 10, the FRF S_{15_z}/I_{10} is shown for both VP transformations, together with a reference. It is clear that with the expanded VPT a more consistent FRF is obtained.

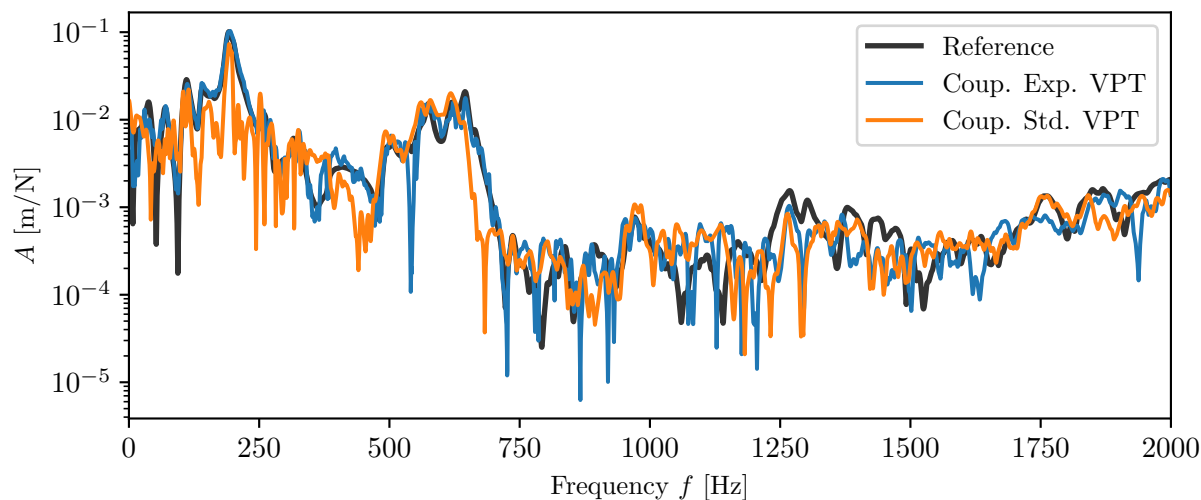


Figure 10: Comparison of the final assembly FRF S_{15_z}/I_{10} obtained with a standard and an expanded VPT, together with a reference measurement.

Similar results can be observed for the FRF S_{15_x}/I_{23} shown in Fig. 11. The coupling results from the rotational accelerometer are in agreement with the reference, especially in the low-frequency range. At higher frequencies the results from standard and expanded VPT are similar. One of the possible reasons is that the assumption of the local rigidity is not completely valid any more and the residual motion (Eq. (8)) after the transformation will contain not only the measurement error (which should be lower for the expanded VPT), but also the flexible motion around the interface. Therefore, both transformations will yield similar results as the primary source of error is the flexibility of the interface.

A close-up view of the low-frequency range for the FRF S_{14_x}/I_{10} is shown in Fig. 12. The coupling results with the expanded VPT are in agreement with the reference compared to the standard VPT. To show the overall quality of the coupling results for both transformations, a coherence criterion (Eq. (12)) is used to compare the coupling and reference results. The frequency-averaged value of the coherence criterion is shown in Fig. 13. It is clear that the expansion of the VPT with a rotational response increases the consistency of the coupling procedure for all the FRFs.

⁵With the three VPs on the TS, a certain level of over-determination can be expected at the interface, since the whole block is in fact rigid in the low-frequency range. Therefore, even a small error in one of the VPTs can lead to erroneous coupling results. Applying a truncated SVD on the interface flexibility $\mathbf{Y}_{\text{int}} = \mathbf{B}\mathbf{Y}^{\text{AIB}}\mathbf{B}^T$ (see Eq. (2)) can be interpreted as a weakening of the interface compatibility, which is advantageous in this configuration.

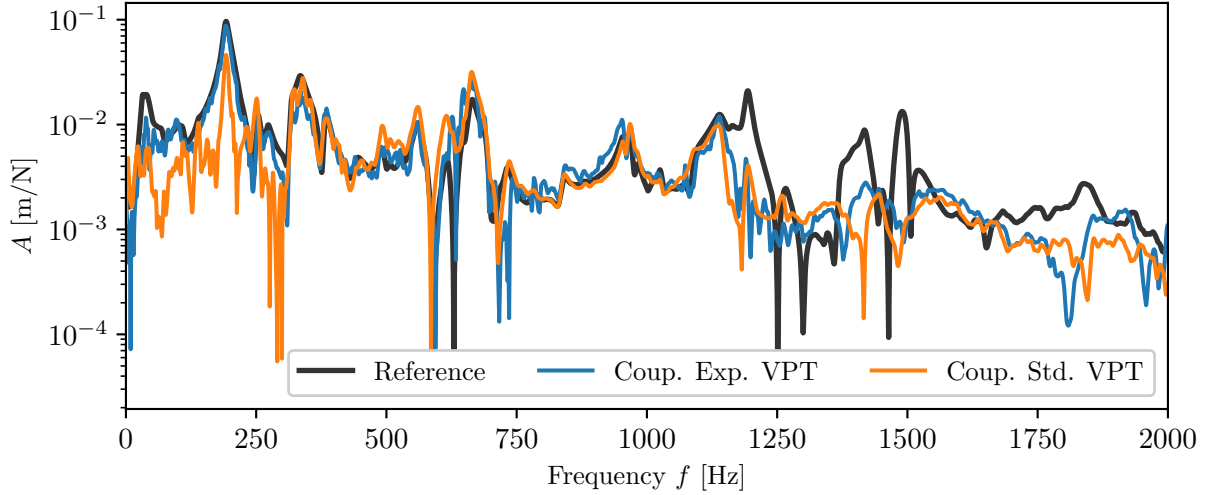


Figure 11: Comparison of the final assembly FRF $S15_x/I23$ obtained with a standard and an expanded VPT, together with a reference measurement.

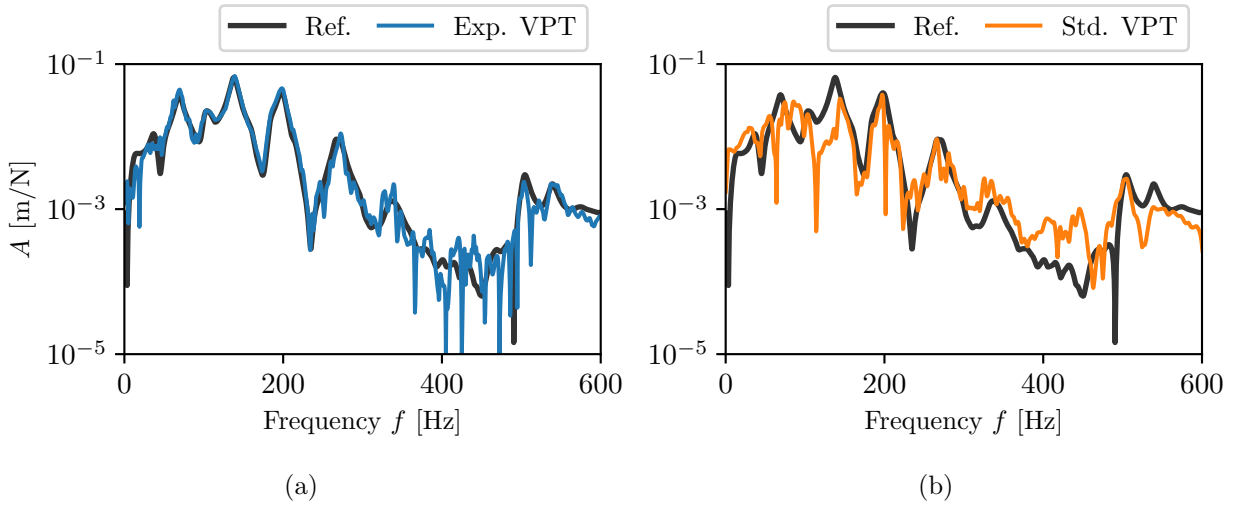


Figure 12: Comparison of the final assembly FRF $S14_x/I10$ with a reference measurement in the low-frequency range: a) expanded VPT; b) standard VPT.

4 Conclusion

Extending the virtual point transformation with a directly measured rotational response can improve the consistency of the coupled FRFs. With the introduction of a rotational weighting matrix in the VPT, the residuals on the rotation and translation sensors are minimized in a comparable norm. With the inclusion of a rotational response, the virtual point transformation can become less sensitive to small deviations in the positions and measurement sensitivity of the sensors. An application of the extended VPT is presented on a test structure, mimicking the dynamics of an engine unit flexibly mounted on a chassis. The coupling results are obtained with the expanded VPT and are compared with the standard VPT. The additional information on the rotational FRFs of the interface yields a more accurate coupling result, which can be observed on all the reference FRFs. Currently, applying the proposed expansion of the VPT is hindered by the scarce availability of rotational accelerometers, as only uni-axial rotational accelerometers are available on the market. Additionally, due to the limited number of rotational accelerometers, the measurements usually cannot be performed within a single measurement campaign, which can be time consuming if a large number of VPs are present in a complex structure.

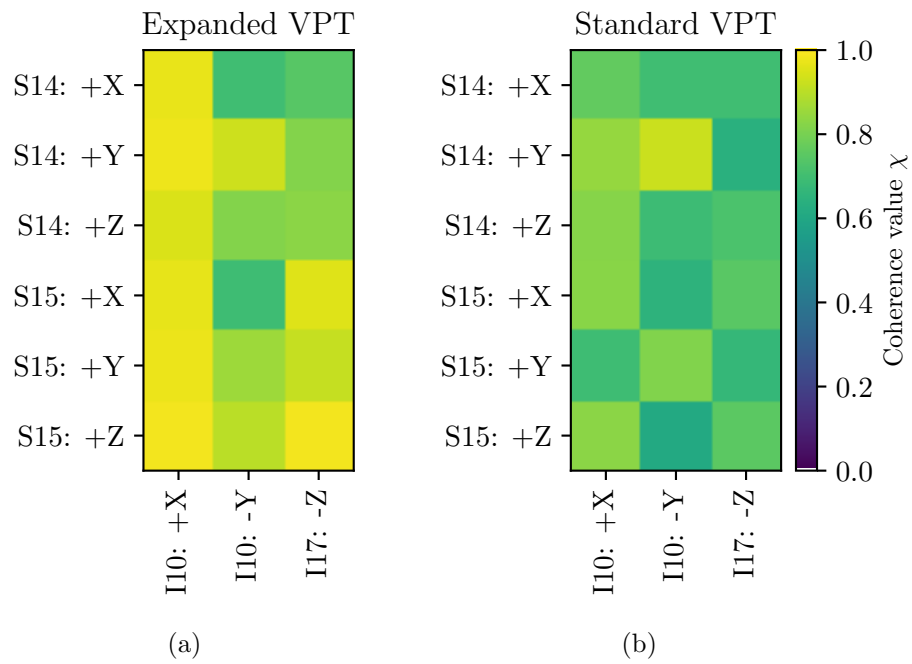


Figure 13: Frequency-averaged value of the coherence criterion between the coupled and reference FRFs: a) expanded VPT; b) standard VPT.

Acknowledgements

The authors acknowledge the partial financial support from the core research funding P2-0263 and applied research project L2-1837, both financed by ARRS, Slovenian research agency.

References

- [1] D. de Klerk, D. J. Rixen, S. N. Voormeeren, General Framework for Dynamic Substructuring: History, Review and Classification of Techniques, *AIAA Journal* 46 (5) (2008) 1169–1181.
- [2] M. S. Allen, D. Rixen, M. van der Seijs, P. Tiso, T. Abrahamsson, R. L. Mayes, *Substructuring in Engineering Dynamics*, Springer International Publishing, 2020.
- [3] A. L. Klosterman, A combined experimental and analytical procedure for improving automotive system dynamics, Ph.D. thesis, University of Cincinnati, Department of Mechanical Engineering (1971).
- [4] J. R. Crowley, A. L. Klosterman, G. T. Rocklin, H. Vold, Direct structural modification using frequency response functions, in: *Proceedings of the 2nd International Modal Analysis Conference, A Conference on Structural Dynamics*.
- [5] B. Jetmundsen, R. L. Bielawa, W. G. Flannely, Generalized Frequency Domain Substructure Synthesis, *Journal of the American Helicopter Society* 33 (1) (1988) 55–64.
- [6] D. de Klerk, D. J. Rixen, J. de Jong, The Frequency Based Substructuring (FBS) Method reformulated according to the Dual Domain Decomposition Method, in: *Proceedings of the 24th International Modal Analysis Conference, A Conference on Structural Dynamics*, (2006).
- [7] M. L. M. Duarte, D. J. Ewins, Some Insights into the Importance of Rotational Degrees-of-freedom and Residual Terms in Coupled Structure Analysis, in: *Proceedings of the 13th International Modal Analysis Conference, A Conference on Structural Dynamics* (1995) 164–170.
- [8] A. Sestieri, P. Salvini, W. D'Ambrogio, Reducing scatter from derived rotational data to determine the frequency response function of connected structures, *Mechanical Systems and Signal Processing* 5 (1) (1991) 25–44.
- [9] D. de Klerk, D. J. Rixen, S. N. Voormeeren, F. Pasteuning, Solving the RDoF Problem in Experimental Dynamic Substructuring, in: *Proceedings of the 26th International Modal Analysis Conference, A Conference on Structural Dynamics*, (2010).
- [10] H. Stefaan, V. der Auweraer Herman, M. Peter, B. Luigi, D. Casagrande, Application of accelerometer-based rotational degree of freedom measurements for engine subframe modelling, in: *Proceedings of the XIX International Modal Analysis Conference, A Conference on Structural Dynamics*.
- [11] M. V. van der Seijs, *Experimental Dynamic Substructuring: Analysis and design strategies for vehicle development*, Ph.D. thesis, TU Delft (2016).
- [12] T. Bregar, N. Holeček, G. Čepón, D. J. Rixen, M. Boltežar, Including directly measured rotations in the virtual point transformation, *Mechanical Systems and Signal Processing* 141 (2020) 106440.
- [13] M. D. Insalaco, The Art of Fabricating Rotational Accelerometer, *Sensors Magazine* (2000).
- [14] E. A. Pasma, M. V. van der Seijs, S. W. B. Klaassen, M. W. van der Kooij, Frequency Based Substructuring with the Virtual Point Transformation, Flexible Interface Modes and a Transmission Simulator, in: *Conference Proceedings of the Society for Experimental Mechanics Series 4* (2018) 205–213.
- [15] M. Haeussler, S. Sendlbeck, D. Rixen, Automated correction of sensor orientation in experimental dynamic substructuring, in: *Dynamics of Coupled Structures, Volume 4*, Springer International Publishing, 2018, pp. 65–70.
- [16] A. Drozg, J. Rogelj, G. Čepón, M. Boltežar, On the performance of direct piezoelectric rotational accelerometers in experimental structural dynamics, *Measurement* 98 (2018) 292–298.
- [17] A. Drozg, G. Čepón, M. Boltežar, Full-degrees-of-freedom frequency based substructuring, *Mechanical Systems and Signal Processing* 127 (2018) 570–579.
- [18] M. van der Seijs, D. van den Bosch, D. Rixen, D. de Klerk, An improved methodology for the virtual point transformation of measured frequency response functions in dynamic substructuring, in: *Proceedings of the 4th International Conference on Computational Methods in Structural Dynamics and Earthquake Engineering (COMPdyn 2013)*, Institute of Structural Analysis and Antiseismic Research School of Civil Engineering National Technical University of Athens (NTUA) Greece, 2014.
- [19] A. El Mahmoudi, F. Trainotti, K. Park, D. J. Rixen, in-situ tpa for nvh analysis of powertrains: An evaluation on an experimental test setup, in: *AAC 2019 : Aachen Acoustics Colloquium/Aachener Akustik Kolloquium, Aachener Akustik Kolloquium 2019, Aachen (Germany), 25 Nov 2019 - 27 Nov 2019, Aachen, 2019*.
- [20] M. S. Allen, R. L. Mayes, E. J. Bergman, Experimental modal substructuring to couple and uncouple substructures with flexible fixtures and multi-point connections, *Journal of Sound and Vibration* 329 (23) (2010) 4891–4906.
- [21] R. Mayes, M. Ross, Advancements in hybrid dynamic models combining experimental and finite element substructures, *Mechanical Systems and Signal Processing* 31 (2012) 56–66.
- [22] D. Otte, J. Leuridan, H. Grangier, R. Aquilina, Prediction of the dynamics of structural assemblies using measured frf-data: some improved data enhancement techniques, in: *Proceedings of the 9th International Modal Analysis Conference, A Conference on Structural Dynamics*, (1991).